

Contrasting pressure evolutions of f electron hybridized states in CeRhIn_5 and YbNi_3Ga_9 : an optical conductivity study

H. Okamura*

Graduate School of Advanced Technology and Science,

Tokushima University, Tokushima 770-8506, Japan

A. Takigawa and T. Yamasaki

Graduate School of Science, Kobe University, Kobe 657-8501, Japan

E. D. Bauer

Los Alamos National Laboratory, Los Alamos, NM 87545, USA

S. Ohara

Graduate School of Engineering, Nagoya Institute of Technology, Nagoya 466-8585, Japan

Y. Ikemoto and T. Moriwaki

Japan Synchrotron Radiation Research Institute, Sayo 679-5198, Japan

(Dated: October 17, 2019)

Abstract

Optical conductivity [$\sigma(\omega)$] of CeRhIn₅ and YbNi₃Ga₉ have been measured at external pressures to 10 GPa and at low temperatures to 6 K. Regarding CeRhIn₅, at ambient pressure the main feature in $\sigma(\omega)$ is a Drude peak due to free carriers. With increasing pressure, however, a characteristic mid-infrared (mIR) peak rapidly develops in $\sigma(\omega)$, and its peak energy and width increase with pressure. These features are consistent with an increased conduction (*c*)-*f* electron hybridization at high pressure, and show that the pressure has tuned the electronic state of CeRhIn₅ from very weakly to strongly hybridized ones. As for YbNi₃Ga₉, in contrast, a marked mIR peak is observed already at ambient pressure, indicating a strong *c*-*f* hybridization. At high pressures, however, the mIR peak shifts to lower energy and becomes diminished, and seems merged with the Drude component at 10 GPa. Namely, CeRhIn₅ and YbNi₃Ga₉ exhibit some opposite tendencies in the pressure evolutions of $\sigma(\omega)$ and electronic structures. These results are discussed in terms of the pressure evolutions of *c*-*f* hybridized electronic states in Ce and Yb compounds, in particular in terms of the electron-hole symmetry often considered between Ce and Yb compounds.

PACS numbers: 75.30.Mb,74.70.Tx,74.62.Fj,78.30.-j

I. INTRODUCTION

Physics of strongly correlated *f*-electron systems, most typically Ce-based and Yb-based intermetallic compounds, has attracted much interest for the last few decades.¹ Central to the problem is a duality between localized and delocalized characteristics exhibited by the *f* electrons. The *f* electrons intrinsically exhibit localized characteristics since the *f* orbitals are located closer to the nucleus than the conduction states. However, they may become partially delocalized by hybridizing with conduction (*c*) electrons. This *c-f* hybridization leads to various interesting phenomena such as the Kondo effect, heavy fermion (HF) formation, intermediate valence (IV), Rudermann-Kittel-Kasuya-Yoshida interaction and the associated magnetic ordering. It also plays an important role in the quantum critical phenomena (QCP) at the border of magnetic ordering.

In IV compounds, the *c-f* hybridization is fairly strong, and the average Ce or Yb valence significantly deviates from 3 and takes an intermediate value well above and below 3 for Ce and Yb compounds, respectively.^{2,3} Optical conductivity [$\sigma(\omega)$] studies have provided much information about their microscopic electronic states.⁴ A marked mid-infrared (mIR) peak has been commonly observed in $\sigma(\omega)$ of many Ce- and Yb-based IV metals, and its origin has been discussed in terms of the *c-f* hybridized electronic states.⁵⁻¹⁷ For example, a model of “renormalized *c-f* hybridized bands” has been used to understand the mIR peak.⁶⁻¹⁰ In this model, a flat *f* band renormalized by large *f* electron correlation (*U*) hybridizes with a wide *c* band, forming a pair of hybridized bands near the Fermi level (E_F).¹⁸⁻²⁰ The mIR peak in this model results from optical excitations between the two bands.⁶ Its peak energy is given as $E_{\text{mIR}} \simeq 2\tilde{V}$, where \tilde{V} is the *c-f* hybridization renormalized by large *U*, and expressed as

$$\tilde{V} \simeq \sqrt{T_K W}, \quad (1)$$

where T_K and W indicate the Kondo temperature and *c* bandwidth, respectively.¹⁸⁻²⁰ Measured E_{mIR} values of different IV metals have been compared with their $\sqrt{T_K W}$ (or related quantities) estimated by other experiments, and a universal relation between E_{mIR} and $\sqrt{T_K W}$ has been found over a variety of Ce and Yb compounds.⁸⁻¹¹ An example of such universal relation¹⁰ is shown in Fig. 1. This universal relation may be regarded as an optical

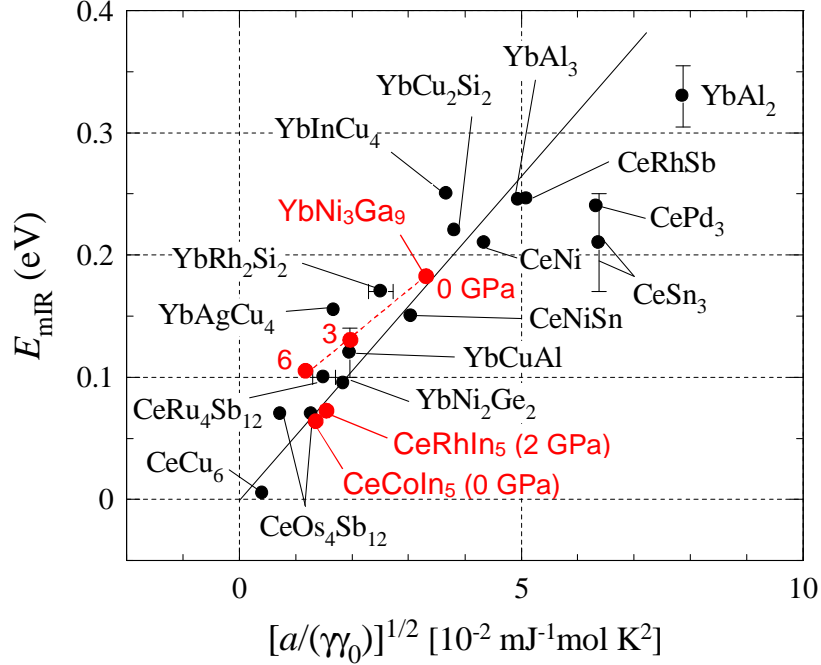


FIG. 1. (Color online) A universal relation between the optical conductivity and the *c-f* hybridization energy observed for Ce and Yb compounds (the red data points have been newly added here, while the others have been reproduced from Ref. 10). Here, the mid-IR peak energy (E_{mIR}) measured for these compounds are plotted as a function of their $\sqrt{a/(\gamma\gamma_0)}$, where γ and γ_0 are the specific heat coefficients of the Ce (Yb) and La (Lu) compounds, respectively, and a is a *f*-degeneracy dependent constant.¹⁰ Here, $\sqrt{a/(\gamma\gamma_0)}$ is a measure of the *c-f* hybridization energy \tilde{V} , through the relation $2\tilde{V} \simeq \sqrt{T_K W} \propto \sqrt{(a/\gamma)(1/\gamma_0)}$. The solid line is guide to the eye.

analogue to the well known Kadowaki-Woods relation.^{21,22} More detailed analyses including effects of *f* level degeneracy and/or the band structure have also been reported.¹²⁻¹⁶ These studies suggest that the *c-f* hybridized band model is an oversimplification for the actual IV metals. For example, it has been suggested that, for Ce compounds, E_{mIR} should correspond to the energy separation from the *c-f* hybridized band below E_F to the bare *f* states above E_F .¹⁶ In fact, the observed E_{mIR} values of some IV compounds seem too large to result between the *c-f* hybridized bands, and such a model may offer a useful alternative to the *c-f* hybridized band model. Nevertheless, it is still true that the mIR peak energy is roughly scaled with $\sqrt{T_K W}$ over many IV metals.⁸⁻¹¹ Clearly, the characteristics of the mIR peak involve the Kondo physics, and are not due to accidental band structures. Furthermore,

effects of momentum-dependent c - f hybridization have been considered in analyzing $\sigma(\omega)$ of Ce compounds.¹⁷

Note that both Ce- and Yb-based IV metals seem to follow the same universal relation,^{10,11} as seen in Fig. 1. For Ce^{3+} and Yb^{3+} ions, their respective f^1 and f^{13} configurations have an electron-hole (e - h) symmetry, since f^{13} is equivalent to h^1 . It has been an important question as to what degree this e - h symmetry is reflected on the properties of Ce and Yb compounds. An example of common property between them, which is consistent with the e - h symmetry, is the formation of HF state with large effective mass. However, Ce and Yb compounds also exhibit noted differences.^{23,24} A useful experimental technique to examine the e - h symmetry is the application of an external pressure (P).²³⁻²⁶ Since Ce^{4+} (f^0) and Yb^{3+} (f^{13}) ions have smaller ionic radii than Ce^{3+} (f^1) and Yb^{2+} (f^{14}) ions, respectively, an applied P generally increases the average valence (v) of Ce toward 4 and that of Yb toward 3. For both Ce and Yb cases, P should also increase the bare (unrenormalized) c - f hybridization, since a reduced interatomic distance should increase the overlap between the c and f wave functions. For Ce compounds, an increase of c - f hybridization with P has been observed, for example, by an increase in T_K .²³ Then, in Fig. 1, upon applying P , a Ce compound should move to upper right. For Yb compounds, in addition to v increases, effective mass increases and magnetic order have been found at high P .^{23,24,26} Namely, Yb compounds seem to exhibit more localized f electron states at high P . This suggests a reduced T_K , and hence a reduced \tilde{V} from Eq. (1), although the bare hybridization in a Yb compound should increase with P as explained above. Therefore, it is intriguing how an Yb compound should move with P in Fig. 1.

In this work, we have addressed the above questions by studying the $\sigma(\omega)$ of CeRhIn_5 and YbNi_3Ga_9 at P to 10 GPa and at temperatures (T) to 6 K. These compounds have attracted much attention for their remarkable properties at high P , as summarized in Fig. 2. CeRhIn_5 exhibits an antiferromagnetism (AF) at $P=0$ with a Neel temperature (T_N) of 3.3 K and an electronic specific heat coefficient of $\gamma= 420 \text{ mJ/K}^2\text{mol}$ above T_N .²⁷ With increasing P , the AF is gradually suppressed, and near a critical pressure (P_c) of ~ 2 GPa, a superconductivity with a transition temperature (T_c) of 2.1 K is observed.^{27,28} Around P_c , various anomalous properties related with QCP have been observed.²⁹⁻³² $\sigma(\omega)$ of CeRhIn_5 at ambient P has already been measured and analyzed in detail,^{17,33} but $\sigma(\omega)$ at high P had not been explored yet. YbNi_3Ga_9 , in contrast, is a paramagnetic IV compound at $P=0$ with $\gamma=30 \text{ mJ/K}^2\text{mol}$,

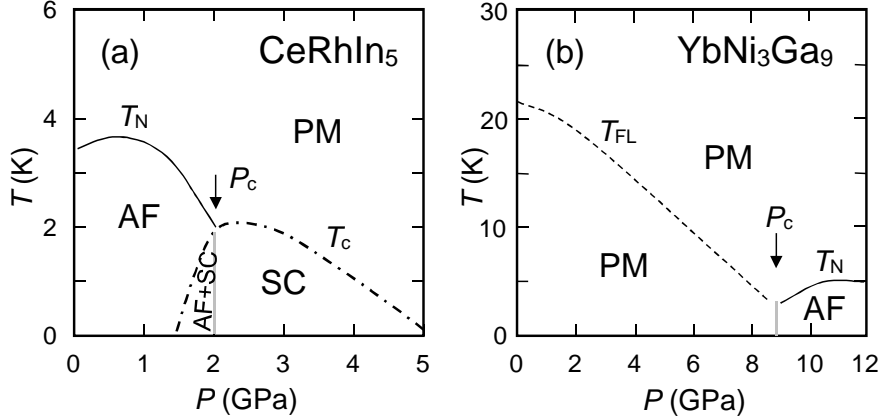


FIG. 2. Schematic phase diagrams of (a) CeRhIn₅ (after Ref. 32) and (b) YbNi₃Ga₉ (after Ref. 36) as functions of temperature (T) and external pressure (P). AF: antiferromagnetic, PM: paramagnetic, SC: superconducting, T_N : Neel temperature, T_c : superconducting transition temperature, T_{FL} : the temperature below which Fermi liquid characteristics are observed, P_c : critical pressure where AF ordering appears or disappears.

indicating a strong c - f hybridization.^{34,35} With increasing P , the measured v increases from 2.6 at $P=0$ to 2.88 at $P=16$ GPa, and an AF state appears above $P_c \simeq 9$ GPa.³⁶ In addition, γ increases significantly with P , reaching $\gamma=1$ J/K²mol at 9 GPa.³⁷ Namely, with increasing P , CeRhIn₅ shows a crossover from localized to delocalized electronic states, while YbNi₃Ga₉ shows that from delocalized to localized ones. Although the lowest T 's in our study, 6 K for CeRhIn₅ and 8 K for YbNi₃Ga₉, are above T_c and T_N , our study should still provide important information about the P tuning of the underlying c - f hybridized state behind the QCP-related properties below T_c and T_N . The mIR peaks of CeRhIn₅ and YbNi₃Ga₉ have indeed shown quite contrasting P evolutions, which are discussed in terms of the c - f hybridized electronic states at high P , and in terms of the e - h symmetry.

II. EXPERIMENTAL

The samples of CeRhIn₅ and YbNi₃Ga₉ used were single crystals grown with self-flux method. The reflectance spectrum [$R(\omega)$] of a sample was measured on an as-grown surface without polishing. $\sigma(\omega)$ was derived from $R(\omega)$ using the Kramres-Kronig (KK) analysis.³⁸ $R(\omega)$ at $P=0$ was measured at photon energies between 15 meV and 30 eV covered by several

light sources,³⁹ including the vacuum uv synchrotron radiation at the beamline BL7B of the UVSOR Facility.⁴⁰ $R(\omega)$ spectra at high P were measured using a diamond anvil cell (DAC).⁴¹ Type IIa diamond anvils with 0.8 mm culet diameter and a stainless steel gasket were used to seal the sample with glycerin as the pressure transmitting medium.^{42–44} A flat surface of a sample was closely attached on the culet surface of the diamond anvil, and $R(\omega)$ at the sample/diamond interface was measured. Small ruby pieces were also sealed to monitor the pressure via its fluorescence. A gold film was placed between the gasket and anvil as a reference of $R(\omega)$. In the KK analysis of $R(\omega)$ measured with DAC, the refractive index of diamond ($n_d=2.4$) was taken into account as previously discussed.⁴⁵ $R(\omega)$ at high P and low T were measured at photon energies from 25 meV (CeRhIn_5) or 20 meV (YbNi_3Ga_9) to 1.1 eV, using synchrotron radiation as a bright IR source⁴⁶ at the beamline BL43IR of SPring-8.^{47,48} Below the measured energy range, $R(\omega)$ was extrapolated with the Hagen-Rubens function.³⁸ More details of the high pressure IR experiments can be found elsewhere.⁴¹

III. RESULTS AND DISCUSSIONS

A. $R(\omega)$ and $\sigma(\omega)$ of CeRhIn_5 at high pressures

Figure 3(a) shows $R(\omega)$ and $\sigma(\omega)$ of CeRhIn_5 at $P=0$ and $T=295$ K over the entire measured spectral range. $R(\omega)$ below 0.3 eV is very high, which indicates highly metallic characteristics of CeRhIn_5 . $\sigma(\omega)$ has a Drude component rising toward zero energy, which is due to free carrier dynamics. Figures 3(b) and 3(c) show $R(\omega)$ and $\sigma(\omega)$ measured at different values of P and T . At $P=0$, $R(\omega)$ and $\sigma(\omega)$ have only minor T dependences, which is consistent with the previous report.³³ With increasing P , as shown in Figs. 3(b) and 3(c), a dip appears and develops in $R(\omega)$, and a pronounced mIR peak develops in $\sigma(\omega)$. At 2 GPa, the mIR peak is barely visible at 295 K, but becomes very pronounced with cooling to 6 K. As discussed in Introduction, such a mIR peak is a hallmark of the c - f hybridized state in Ce compounds. Namely, CeRhIn_5 at 2 GPa has much stronger c - f hybridization than at 0 GPa. Note that the T -evolution of mIR peak at $P=2$ GPa is strikingly similar to that of CeCoIn_5 at $P=0$, with very close E_{mIR} .^{33,50,51} CeCoIn_5 at $P=0$ is also a superconductor with almost the same T_c as that of CeRhIn_5 at 2 GPa.⁵⁰ These similarities between CeCoIn_5

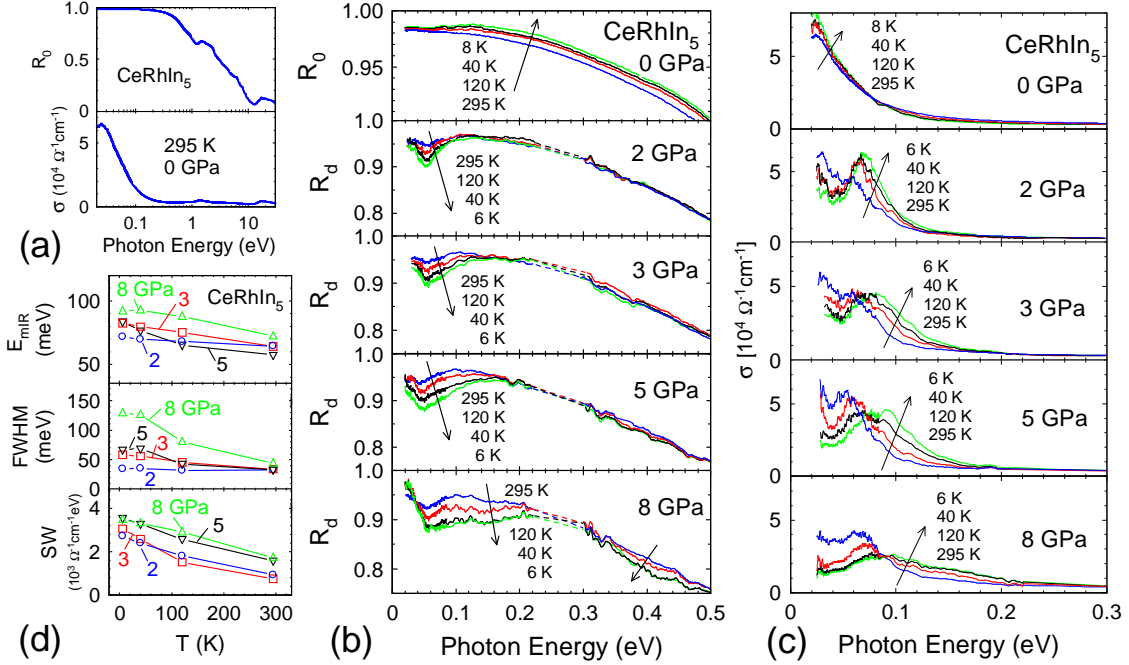


FIG. 3. (Color online) (a) $R(\omega)$ and $\sigma(\omega)$ spectra of CeRhIn₅ measured at $T=295$ K and $P=0$. (b) $R(\omega)$ at $P=0$, 2, 3, 5, and 8 GPa and at $T=295$ K (blue curves), 120 K (red), 40 K (black), and 8 K (0 GPa) or 6 K (2-8 GPa) (green). R_0 and R_d denote $R(\omega)$ measured at sample/vacuum and sample/diamond interfaces, respectively. The broken-curve portions of the spectra indicate interpolations, which were needed because of strong absorption by the diamond.⁴⁹ (c) $\sigma(\omega)$ at the same values of P and T as in (b). (d) Peak position (E_{mIR}), the full width at half maximum (FWHM), and the spectral weight (SW) of the mIR peak in $\sigma(\omega)$, given by the spectral fitting.

at 0 GPa and CeRhIn₅ at 2 GPa indicate that their c - f hybridized electronic states are also similar. In Fig. 1, E_{mIR} of CeCoIn₅ at 0 GPa and CeRhIn₅ at 2 GPa have been added using their γ and γ_0 data.⁵² Clearly, they follow the universal relation well, and their plots are indeed close to each other reflecting their similarity. At $P=3$ GPa, the mIR peak of CeRhIn₅ is broader than that at 2 GPa. This broadening of the mIR peak should basically indicate a broadening of the f band, and hence a stronger c - f hybridization. From the evolutions of $\sigma(\omega)$ from $P=0$ to 3 GPa, it is clear that the electronic structure of CeRhIn₅ in the normal state at 6 K changes significantly from very weakly to moderately hybridized ones, which should be an important basis for the QCP observed below 2 K. From 3 to 8 GPa, the mIR peak becomes apparently much broader, and its spectral weight (SW) shifts toward higher

energy. In addition, at 5 and 8 GPa the mIR peak is clearly observed even at room T , which is a feature often observed for IV Ce compounds. Namely, CeRhIn₅ above 5 GPa is likely a strongly hybridized IV compound. Unfortunately, γ data of CeRhIn₅ above 2 GPa are unavailable, so E_{mIR} above 2 GPa cannot be plotted in Fig. 1. However, it is almost certain that the plot for CeRhIn₅ moves to upper right with P , since the resistivity data²⁸ strongly suggest that the hybridization is much stronger at 8 GPa.

To analyze the evolution of mIR peak more quantitatively, we have performed spectral fitting on the measured $\sigma(\omega)$ using the Drude-Lorentz oscillator model.³⁸ Details of the fitting procedures and examples of the fitted spectra are given in the Appendix. In Fig. 3(d), the E_{mIR} , full width at half maximum (FWHM), and the SW of the mIR peak given by the fitting are summarized. The fitting results in Fig. 3(d) confirm the features discussed above, namely the P -induced increases in E_{mIR} , SW, and the width. However, they also reveal that the increases in E_{mIR} and SW are at most about 30 %. In contrast, the increase in the width at 6 K is particularly large from 5 to 8 GPa, suggesting that f electron bandwidth should rapidly increase at this P range.

B. $R(\omega)$ and $\sigma(\omega)$ of YbNi₃Ga₉ at high pressures

Figure 4(a) shows measured $R(\omega)$ and $\sigma(\omega)$ of YbNi₃Ga₉ over a wide energy range at $P=0$ and $T=295$ K, and Figures 4(b) and 4(c) show those below 0.4 eV at different values of P and T . At $P=0$, a dip is observed in $R(\omega)$ at 0.1-0.2 eV range and a mIR peak in $\sigma(\omega)$ at 0.1-0.3 eV range, both of which are strongly T dependent. A Drude component is also observed in $\sigma(\omega)$ below 0.1 eV, which rises steeply toward zero energy. With cooling, the dip becomes deeper, and the mIR peak becomes more pronounced and slightly shifts to higher energy. In addition, a shoulder appears in $\sigma(\omega)$ near 70 meV at low T . Furthermore, the onset of Drude component becomes extremely sharp at low T . This is because $\sigma(0)$ at low T is very large, exceeding $1 \times 10^6 \Omega^{-1}\text{cm}^{-1}$ at 8 K.^{34,36} This extremely narrow Drude component is due to the Drude response of heavy quasiparticles formed at low T .⁵ These features are qualitatively very similar to those previously observed for other Yb-based IV metals such as YbAl₃.⁵⁵ Using the observed $E_{\text{mIR}}=0.18$ eV at 8 K with $\gamma=30$ mJ/K²mol and $\gamma_0=6.3$ mJ/K²mol,³⁴ a plot for YbNi₃Ga₉ at $P=0$ has been added in Fig. 1. Clearly, YbNi₃Ga₉ well follows the universal relation.

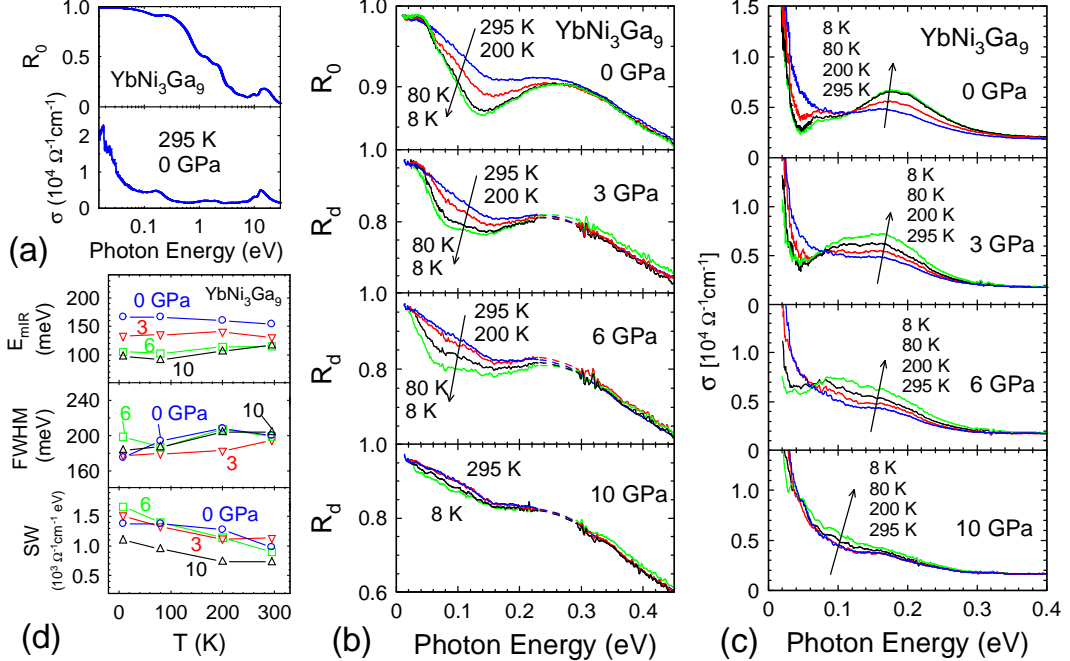


FIG. 4. (Color online) (a) $R(\omega)$ and $\sigma(\omega)$ spectra of $YbNi_3Ga_9$ measured at $T=295$ K and $P=0$. (b) $R(\omega)$ spectra at $P=0$, 3 , 6 , and 10 GPa and at $T=295$ K (blue curves), 200 K (red), 80 K (black) and 8 K (green). The broken curve portions indicate smooth interpolations, as already mentioned in the caption of Fig. 3(b).⁴⁹ (c) $\sigma(\omega)$ spectra at the same values of P and T as those in (b). (d) Results of the spectral fitting, with the same notations as those in Fig. 3(d).

The $\sigma(\omega)$ spectra at various values of T and P have been analyzed by spectral fitting, similarly to those of $CeRhIn_5$. The results are summarized in Fig. 4(d), and examples of the fitting are given in Appendix. At 3 GPa, $R(\omega)$ and $\sigma(\omega)$ spectra are still strongly T dependent. Note that, at low T , the mIR peak seems to consist of two peaks, located at ~ 0.1 and ~ 0.17 eV. A similar two-peak feature is also observed at 6 GPa. The origins for the two peaks are unclear, hence we define E_{mIR} as the center-of-mass position of the Lorentz oscillators used to fit the mIR peak. As indicated in Fig. 4(d), the obtained E_{mIR} decreases with P from 0 to 3 GPa, and also from 3 to 6 GPa. The E_{mIR} 's at $P=3$ and 6 GPa and $T=8$ K given by the spectral fitting have been added in Fig. 1, using the γ data measured at high P .^{37,59} The plot for $YbNi_3Ga_9$ moves to down left with P , namely, it actually moves in an opposite manner to that of Ce compounds. At 10 GPa, the mIR peak seems much weaker than at 6 GPa, and almost merged with the Drude component. The remaining mIR

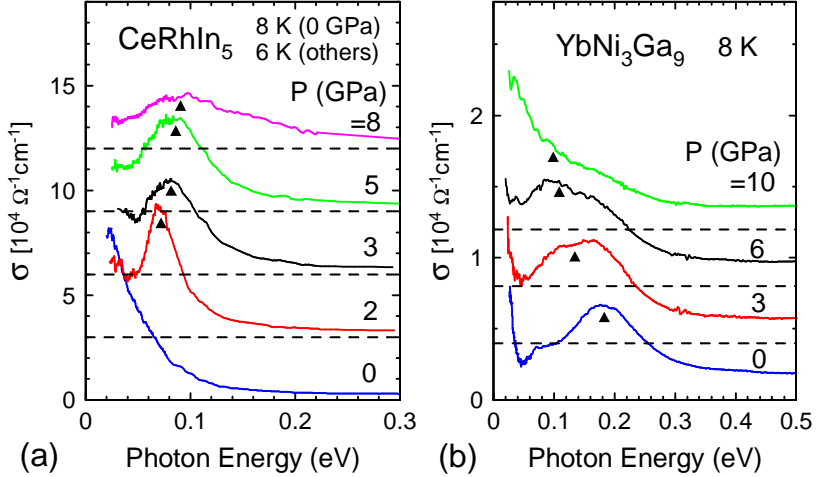


FIG. 5. (Color online) Comparison of P evolutions of $\sigma(\omega)$ at low T between (a) CeRhIn₅ and (b) YbNi₃Ga₉. The spectra are vertically offset for clarity, and the triangles indicate the E_{mIR} values.

component has been evaluated by the fitting as in Fig. 4(d), which indicates that E_{mIR} further decreases compared with that at 6 GPa. From Figs. 4(b) and 4(c), the T variations of $R(\omega)$ and $\sigma(\omega)$ at 10 GPa are much smaller than those at 6 GPa. This strongly suggests that the T -dependent hybridization has become much weaker with P from 6 to 10 GPa. This is reasonable since the f electron state should be more localized and less hybridized above $P_c \sim 9$ GPa, where an AF state appears below $T_N=5$ K. The fitting results in Fig. 4(d) also indicate that E_{mIR} does not change much with T , although it clearly decreases with P . In addition, the peak width seems to exhibit no systematic changes with T and P .

C. Comparison of pressure evolutions between CeRhIn₅ and YbNi₃Ga₉

To compare more clearly the observed P evolutions of $\sigma(\omega)$ between CeRhIn₅ and YbNi₃Ga₉, the $\sigma(\omega)$ spectra at the lowest measured T are displayed in Fig. 5. Clearly, the P evolutions of CeRhIn₅ and YbNi₃Ga₉ have some contrasting and opposite tendencies: With increasing P , the mIR peak of CeRhIn₅ appears and grows, and shifts to higher energy. In contrast, the mIR peak of YbNi₃Ga₉ is well developed already at $P=0$, and shifts to lower energy with P and becomes diminished at 10 GPa. On the other hand, not all the P evolutions of mIR peak exhibit opposite tendencies between them. For example, the mIR peak width of CeRhIn₅ significantly increases with P , but that of YbNi₃Ga₉ does not

exhibit a narrowing or any other systematic change, as indicated in Fig. 6(b). In addition, P -induced shift of E_{mIR} seems much larger for YbNi_3Ga_9 than for CeRhIn_5 . Below, we consider these results in terms of the P evolution of IV states in Ce and Yb compounds.

In a Ce compound with $v=3$ and completely localized f^1 state, $\sigma(\omega)$ should consist only of a Drude component due to c electrons, since the system is a metal where the localized f electrons do not contribute to the Drude response. This applies well to CeRhIn_5 at 0 GPa, since its $\sigma(\omega)$ has only a Drude component in Fig 3(c) and its v should be very close to 3. As stated in Introduction, an external P on a Ce compound should increase v from 3. In this IV state, $\sigma(\omega)$ would exhibit a mIR peak due to the hybridized state, as actually observed in $\sigma(\omega)$ of CeRhIn_5 at 2 and 3 GPa. With further increasing P , both the energy and width of the mIR peak should increase, since the hybridization and f bandwidth increase with P . This is again consistent with the observed $\sigma(\omega)$ at 3-8 GPa. Namely, the observed P evolutions of $\sigma(\omega)$ for CeRhIn_5 seem quite consistent with those expected for a Ce compound. P -induced higher-energy shifts and development of an IR peak in $\sigma(\omega)$ have also been observed for $\text{CeRu}_4\text{Sb}_{12}$ (Ref. 57) and CeIn_3 .⁵⁸

As for Yb compounds, as stated in Introduction, an ionic radius consideration suggests that v of an IV Yb compound should increase toward 3 with P . In the limit of exactly $v=3$ state with completely localized f^{13} state, $\sigma(\omega)$ would consist only of a broad Drude component due to c electrons, similarly to the f^1 (Ce^{3+}) case. Namely, the main feature in $\sigma(\omega)$ of an IV Yb compound should evolve from a mIR peak at $P=0$ into a broad Drude component in the limit of very high P . Clearly, such a P evolution is qualitatively consistent with that observed for YbNi_3Ga_9 in Fig. 5(b): $\sigma(\omega)$ has a well developed mIR peak at $P=0$, which shifts to lower energy with P and becomes much weaker at 10 GPa. $\sigma(\omega)$ at 10 GPa actually looks like a broad Drude component, and the residual mIR peak SW would become even weaker if P is further increased since v still increases from 2.84 at 10 GPa to 2.88 at 16 GPa.³⁶

The discussions above indicate that the opposite tendencies in the P evolutions of $\sigma(\omega)$ between CeRhIn_5 and YbNi_3Ga_9 , including the opposite P -induced moves in Fig. 1, are consistent with the consideration of ionic radius and e - h symmetry under high P . The expression for the renormalized hybridization \tilde{V} in Eq. (1) has been derived for an f^1 (Ce^{3+}) system,¹⁸⁻²⁰ but is also valid for h^1 (f^{13} , Yb^{3+}) system under the e - h symmetry. Hence, for both Ce and Yb compounds, \tilde{V} and E_{mIR} should become smaller with increasing localization

and decreasing T_K . This has been actually demonstrated by the Ce and Yb compounds plotted in Fig. 1. Then, according to Eq. (1), the P -induced decrease of E_{mIR} for YbNi_3Ga_9 indicates that \tilde{V} decreases with P , although the bare (unrenormalized) hybridization should increase with P as already discussed. This peculiar property of an Yb compound has been discussed⁶¹ in terms of the c - f exchange energy, J_{cf} , expressed as⁶²

$$J_{cf} \simeq \frac{|V|^2}{|E_F - \epsilon_f|}, \quad (2)$$

where V is the bare c - f hybridization averaged over the k space and ϵ_f is the one-electron (unrenormalized) f level. Eq. (2) has been derived for an f^1 system with sufficiently large U , but is also valid for h^1 system under the e - h symmetry. J_{cf} is related with T_K as $T_K \simeq W \exp(-W/J_{cf})$. Note that $|V|$ in Eq. (2) increases with P for both Ce and Yb cases, as discussed earlier. In addition, note that ϵ_f should increase with P relative to E_F .^{61,63} For Ce case, ϵ_f is located below E_F and approaches E_F with increasing P . Hence $|E_F - \epsilon_f|$ decreases in Eq. (2), so that J_{cf} increases with P . For Yb case, in contrast, ϵ_f is the f hole level located above E_F , and moves away from E_F with P . Hence $|E_F - \epsilon_f|$ increases with P in Eq. (2), so that J_{cf} may either increase or decrease depending on which of $|E_F - \epsilon_f|$ and $|V|^2$ increases more. Therefore, the P -induced decrease of E_{mIR} for YbNi_3Ga_9 suggests that $|E_F - \epsilon_f|$ increases with P more than $|V|^2$ does.

As already mentioned, some of the observed P evolutions of $\sigma(\omega)$ are not opposite or symmetrical between CeRhIn_5 and YbNi_3Ga_9 . For example, the mIR peak of CeRhIn_5 shows progressive and significant broadenings with P , while that of YbNi_3Ga_9 does not show a narrowing or any systematic change with P . In addition, P -induced shift of E_{mIR} seems much larger for YbNi_3Ga_9 (0.18 to 0.1 eV on going from 0 to 6 GPa) than for CeRhIn_5 (70 to 90 meV on going from 2 to 8 GPa). Microscopic mechanisms for these results are unclear, but they should involve microscopic differences between Ce^{3+} and Yb^{3+} not considered in the simple e - h symmetry argument. For example, the $4f$ orbital of Yb^{3+} is much more localized than that of Ce^{3+} , leading to a much smaller f bandwidth and $|V|$ for Yb^{3+} .^{23,24} In addition, the spin-orbit splitting of Yb^{3+} (~ 1.3 eV) is much larger than that of Ce^{3+} (~ 0.3 eV). It has been pointed out^{23,24} that, due to these differences, the P -induced variation of v from 3.0 in a Ce compound should be at most to ~ 3.16 , while that in an Yb compound can be changed more widely between 2 and 3. Experimentally, v of CeRhIn_5 at high P has not been reported, but that of CeCoIn_5 has been reported to vary from 3.00 at $P=0$

to 3.05 at 8 GPa.⁶⁰ On the other hand, v of YbNi_3Ga_9 varies from 2.60 at $P=0$ to 2.84 at $P=10$ GPa.³⁶ These different ranges of variation in v may be related to the much larger P -induced shifts of E_{mIR} for YbNi_3Ga_9 , since v is closely related with T_{K} and \tilde{V} . To further understand P evolutions of $\sigma(\omega)$ and electronic structures for Yb compounds, more studies on other Yb-based IV compounds are clearly needed. For example, YbCu_2Ge_2 (Ref. 64) and YbAl_2 (Ref. 65) are other examples that exhibit large P dependences in their physical properties. $\sigma(\omega)$ studies of these compounds at high P are in progress.⁶⁶

IV. SUMMARY

$\sigma(\omega)$ studies of CeRhIn_5 and YbNi_3Ga_9 at high P have been performed to probe the P evolutions of their c - f hybridized electronic structures. The main feature in the measured $\sigma(\omega)$ is a mIR peak, which has exhibited many opposite or symmetrical P evolutions between CeRhIn_5 and YbNi_3Ga_9 : With increasing P , the mIR peak develops and shifts to higher energy for CeRhIn_5 , while it shifts to lower energy and becomes diminished at high P for YbNi_3Ga_9 . These results are qualitatively consistent with the e - h symmetry and P -induced variations in the Ce and Yb ionic radii. However, YbNi_3Ga_9 has also exhibited P evolutions of mIR peak not opposite to those of CeRhIn_5 , which are likely due to microscopic differences between Ce and Yb not included in the simple e - h symmetry arguments.

ACKNOWLEDGMENTS

H. O. would like to thank Dr. Takeshi Mito and Dr. Tetsuya Mutou for useful discussions. The experiments at SPring-8 were performed under the approval by JASRI (2011B0089, 2012A0089, 2012B0089, 2013A0089, 2013B0089, 2013B1159), and those at UVSOR under the approval by Institute for Molecular Science. H. O. acknowledges financial support from JSPS KAKENHI (21102512, 23540409, 26400358).

Appendix: Spectral fittings on $\sigma(\omega)$

The spectral fittings were performed using the Drude-Lorentz model.³⁸ In this model, the complex dielectric function is expressed as a sum of Drude and Lorentz oscillators, which

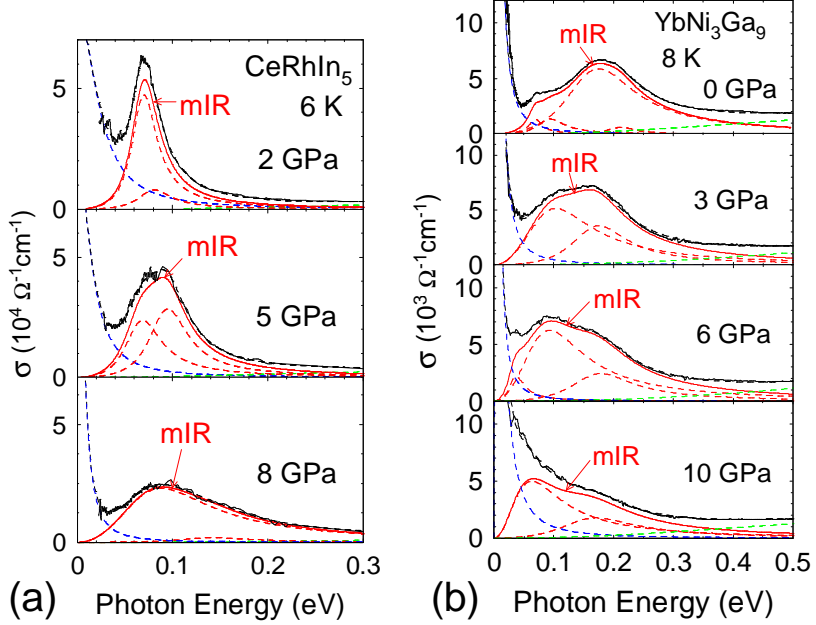


FIG. 6. (Color online) (a) Examples of Drude-Lorentz fitting on $\sigma(\omega)$ of CeRhIn₅ measured at $T=6$ K and at $P=2$, 5, and 8 GPa, and (b) those of YbNi₃Ga₉ measured at 8 K at $P=0$, 3, 6, and 10 GPa, as discussed in the Appendix. Shown in each graph are the measured data (black solid curves), total fit (black broken), Drude component (blue broken), two Lorentz oscillators (red broken), mIR peak (red solid) which is the sum of the Lorentz oscillators, and the background (green broken).

represent free and bound electrons, respectively, as

$$\hat{\epsilon}(\omega) = \epsilon_{\infty} + \sum_j \frac{\omega_{p,j}^2}{\omega_{0,j}^2 - \omega^2 - i\omega\gamma_j}. \quad (\text{A.1})$$

Here, ω_p , ω_0 , and γ are the plasma frequency, natural frequency, and damping, respectively. j denotes the j th oscillator, and $\omega_0=0$ for a Drude oscillator. ϵ_{∞} represents contribution from higher-lying interband transitions. In the fitting, these parameters are adjusted so as to reproduce a measured $\sigma(\omega)$ through the relation $\sigma(\omega) = (\omega/4\pi)\text{Im}(\hat{\epsilon})$.

Figure 6(a) shows examples of fitting for $\sigma(\omega)$ of CeRhIn₅ at 6 K. The measured $\sigma(\omega)$ spectra can be reproduced well by using two Lorentz oscillators for the mIR peak, in addition to a Drude oscillator and a broad Lorentz oscillator peaked at 0.45 eV serving as a background. $\epsilon_{\infty}=5$ is used for all the fitting, and the fitted mIR peak is the sum of the two Lorentz oscillators. Although not shown, $\sigma(\omega)$ at other values of P and T can be fit-

ted similarly. Note that two Lorentz oscillators are used simply because a single Lorentz oscillator is not sufficient to fit the mIR peak, and that the two Lorentz oscillators are not assigned to any specific origins. In addition, due to the use of DAC, the measured spectral range does not cover low-enough energies for fitting the Drude component. However, since our main focus here is the evolution of mIR peak with P and T , the uncertainty regarding the Drude peak fitting is not a serious problem. To reduce the uncertainty in fitting the Drude component, $\sigma(0)$ value given by the fitting was kept in the range $8-20 \times 10^4 \Omega^{-1}\text{cm}^{-1}$, and $\sigma(0)$ was increased with decreasing T . These constraints on the Drude component are implied from the $\sigma(0)$ at $P=0$ [Fig. 3(c)] and also from the measured dc conductivities.²⁷

Figure 6(b) shows examples of fitting for YbNi_3Ga_9 . In some cases more than two Lorentz oscillators are needed to fit the mIR peak reasonably well. A background Lorentz oscillator at 0.75 eV and $\epsilon_\infty=5$ are used. Here, the fitting parameters are chosen so that $\sigma(0)$ at each data matched the measured dc conductivity at the same T and P .^{34,36,56} This procedure greatly reduced the uncertainty in fitting the Drude component. At 0-6 GPa, as mentioned in Section III.B, the Drude component is extremely narrow due to the large values of $\sigma(0)$. At 10 GPa, the mIR peak is not well resolved from the Drude component any more, but the fitting was nevertheless performed to evaluate the remaining mIR component, as shown in Fig. 6(b). Again, measured $\sigma(0)$,³⁶ for example $4.5 \times 10^4 \Omega^{-1}\text{cm}^{-1}$ at $P=10$ GPa and $T=8$ K, were used to reduce the uncertainty. The fitting results suggest that the SW of mIR peak at 10 GPa is still sizable, but is indeed much smaller than that at 6 GPa, as discussed in the main text.

The E_{mIR} , FWHM, and SW of the mIR peak obtained from the fitting are displayed in Figs. 3(d) and 4(d) for CeRhIn_5 and YbNi_3Ga_9 , respectively. Here, E_{mIR} is defined as the center of mass of the Lorentz peaks, namely the mean of ω_0 's of the Lorentz oscillators weighted by their respective SW's. The SW of a Lorentz oscillator is defined as its area in $\sigma(\omega)$, and the SW of the mIR peak is the area of the fitted total mIR peak, namely the red solid curves in Fig. 6.

* Electronic address: ho@tokushima-u.ac.jp

¹ See, for example, Y. Ōnuki, *Physics of Heavy Fermions: Heavy Fermions and Strongly Corre-*

lated Electron Systems (World Scientific, 2018).

² J. Lawrence, Mod. Phys. Lett. B **22**, 1273 (2008).

³ P. S. Riseborough and J. M. Lawrence, Rep. Prog. Phys. **79**, 084501 (2016).

⁴ For a recent review, see, for example, R. Y. Chen and N. L. Wang, Rep. Prog. Phys. **79**, 064502 (2016).

⁵ B. C. Webb, A. J. Sievers, and T. Mihalisin, Phys. Rev. Lett. **57**, 1951 (1986).

⁶ S. R. Garner, J. N. Hancock, Y. W. Rodriguez, Z. Schlesinger, B. Bucher, Z. Fisk, and J. L. Sarrao, Phys. Rev. B **62**, R4778 (2000).

⁷ L. Degiorgi, F. Anders, and G. Gruner, Eur. Phys. J. B **19**, 167 (2001).

⁸ S. V. Dordevic, D. N. Basov, N. R. Dilley, E. D. Bauer, and M. B. Maple, Phys. Rev. Lett. **86**, 684 (2001).

⁹ J. N. Hancock, T. McKnew, Z. Schlesinger, J. L. Sarrao, and Z. Fisk, Phys. Rev. Lett. **92**, 186405 (2004).

¹⁰ H. Okamura, T. Watanabe, M. Matsunami, T. Nishihara, N. Tsujii, T. Ebihara, H. Sugawara, H. Sato, Y. Ōnuki, Y. Ishikawa, T. Takabatake, and T. Nanba, J. Phys. Soc. Jpn. **76**, 023703 (2007).

¹¹ G. Lonzarich, D. Pines, and Y. Yang, Rep. Prog. Phys. **80**, 024501 (2017).

¹² T. Mutou and T. Sasو, J. Phys. Soc. Jpn. **73**, 2900 (2004).

¹³ H. Kuroiwa, Y. Imai, and T. Sasو, J. Phys. Soc. Jpn. **76**, 124704 (2007).

¹⁴ S. Kimura, T. Iizuka, and Y. Kwon, J. Phys. Soc. Jpn. **78**, 013710 (2009).

¹⁵ S. Kimura, Phys. Rev. B **80**, 073103 (2009).

¹⁶ S. Kimura, Y. Kwon, Y. Matsumoto, H. Aoki, and O. Sakai, J. Phys. Soc. Jpn. **85**, 083702 (2016).

¹⁷ K. S. Burch, S. V. Dordevic, F. P. Mena, A. B. Kuzmenko, D. van der Marel, J. L. Sarrao, J. R. Jeffries, E. D. Bauer, M. B. Maple, and D. N. Basov, Phys. Rev. B **75**, 054523 (2007).

¹⁸ D. L. Cox, Phys. Rev. Lett. **58**, 2730 (1987).

¹⁹ P. Coleman, in *Handbook of Magnetism and Advanced Magnetic Materials Vol. 1: Fundamentals and Theory* (Wiley, New York, 2007). Also available as P. Coleman, Heavy Fermions: electrons at the edge of magnetism, arXiv:cond-mat/0612006 (2007).

²⁰ P. Coleman, Heavy fermions and the Kondo lattice: a 21st century perspective, arXiv: 1509.05769 (2015).

²¹ K. Kadokawa and S. B. Woods, Solid State Commun. **58**, 507 (1986).

²² N. Tsujii, H. Kontani, and K. Yoshimura, Phys. Rev. Lett. **94**, 057201 (2005).

²³ J. Flouquet and H. Harima, "Heavy fermion material: Ce versus Yb case", arXiv:0910.3110 (2009). Also published in Japanese in Kotai Butsuri **47**, 47 (2012).

²⁴ G. Knebel, R. Boursier, E. Hassinger, G. Lapertot, P. G. Niklowetz, A. Pourret, B. Salce, J. P. Sanchez, I. Sheikin, P. Bonville, H. Harima, and J. Flouquet, J. Phys. Soc. Jpn. **75**, 114709 (2006).

²⁵ A. V. Goltsev and M. M. Abd-Elmeguid, J. Phys.: Condense. Matter **17**, S813 (2005).

²⁶ J. D. Thompson and J. M. Lawrence, Handbook on the Physics and Chemistry of Rare Earths, Vol. 19 (ed. K.A. Gschneidner, Jr. L. Eyring, G. H. Lander, and G. R. Choppin, Elsevier 1994), p382.

²⁷ H. Hegger, C. Petrovic, E. G. Moshopoulou, M. F. Hundley, J. L. Sarrao, Z. Fisk, J. D. Thompson, Phys. Rev. Lett. **84**, 4986 (2000).

²⁸ T. Muramatsu, N. Tateiwa, T. C. Kobayashi, K. Shimizu, K. Amaya, D. Aoki, H. Shishido, Y. Haga, and Y. Ōnuki, J. Phys. Soc. Jpn. **70**, 3362 (2001).

²⁹ For review, see, for example, J. L. Sarrao and J. D. Thompson, J. Phys. Soc. Jpn. **76**, 051013 (2007), and papers cited therein.

³⁰ H. Shishido, R. Settai, H. Harima, and Y. Ōnuki, J. Phys. Soc. Jpn. **74**, 1103 (2005).

³¹ T. Park, F. Ronning, H. Q. Yuan, M. B. Salamon, R. Movshovich, J. L. Sarrao, and J. D. Thompson, Nature **440**, 65 (2006),

³² G. Knebel, D. Aoki, J.-P. Brison, and J. Flouquet, J. Phys. Soc. Jpn. **77**, 114704 (2008).

³³ F. P. Mena, D. van der Marel, and J. L. Sarrao, Phys. Rev. B **72**, 045119 (2005).

³⁴ T. Yamashita, R. Miyazaki, Y. Aoki, and S. Ohara, J. Phys. Soc. Jpn. **81**, 034705 (2012).

³⁵ Y. Utsumi, H. Sato, S. Ohara, T. Yamashita, K. Mimura, S. Motonami, K. Shimada, S. Ueda, K. Kobayashi, H. Yamaoka, N. Tsujii, N. Hiraoka, H. Namatame, M. Taniguchi, Phys. Rev. B **86**, 115114 (2012).

³⁶ K. Matsubayashi, T. Hirayama, T. Yamashita, S. Ohara, N. Kawamura, M. Mizumaki, N. Ishimatsu, S. Watanabe, K. Kitagawa, Y. Uwatoko, Phys. Rev. Lett. **114**, 086401 (2015).

³⁷ K. Umeo, T. Otaki, Y. Arai, S. Ohara, and T. Takabatake, Phys. Rev. B **98**, 024420 (2018).

³⁸ M. Dressel and G. Grüner, *Electrodynamics of Solids* (Cambridge University Press, Cambridge, 2002).

³⁹ H. Okamura, Chapter 4 in *Optical Techniques for Solid State Materials Characterization* (R. Prasankumar and A. Taylor, Ed.), CRC Press (2011).

⁴⁰ K. Fukui, H. Miura, H. Nakagawa, I. Shimoyama, K. Nakagawa, H. Okamura, T. Nanba, M. Hasumoto, and T. Kinoshita, Nucl. Instr. Methods Phys. Res. A **467-468**, 601 (2001).

⁴¹ H. Okamura, Y. Ikemoto, T. Mariwaki, and T. Nanba, Jpn. J. Appl. Phys. **56**, 05FA11 (2017).

⁴² N. Tateiwa and Y. Haga, Rev. Sci. Instrum. **80**, 123901 (2009).

⁴³ S. Klotz, K. Takemura, Th. Strassie, and Th. Hansen, J. Phys.: Condens. Matter **24**, 325103 (2012).

⁴⁴ Glycerin has good characteristics as a pressure transmitting medium.^{42,43} It does not solidify at room T up to about 5 GPa, and produces more hydrostatic pressure even at lower T compared with solid media such as NaCl and KBr, which are commonly used for optical studies with DAC. Therefore, we have used glycerin although using a liquid medium such as glycerin in a $R(\omega)$ study with DAC is technically much more challenging than using a solid medium.

⁴⁵ H. Okamura, J. Phys. Conf. Ser. **359**, 012013 (2012).

⁴⁶ S. Kimura and H. Okamura, J. Phys. Soc. Jpn. **82**, 021004 (2013).

⁴⁷ Y. Ikemoto, T. Moriwaki, T. Hirono, S. Kimura, K. Shinoda, M. Matsunami, N. Nagai, T. Nanba, K. Kobayashi, and H. Kimura, Infrared Phys. Tech. **45**, 369 (2004).

⁴⁸ T. Moriwaki and Y. Ikemoto, Infrared Phys. Tech. **51**, 400 (2008).

⁴⁹ Due to strong absorption by the diamond anvil, the spectral range between 0.23 and 0.3 eV could not be measured well. Therefore, the $R(\omega)$ spectra in this range were interpolated as indicated by the broken curves in Figs. 3(b) and 4(b). It is clear from Figs. 3(c) and 4(c) that these interpolations have only minor effects on the obtained $\sigma(\omega)$.

⁵⁰ E. J. Singley, D. N. Basov, E. D. Bauer, and M. B. Maple, Phys. Rev. B **65**, 161101(R) (2002).

⁵¹ H. Okamura, A. Takigawa, E. D. Bauer, T. Moriwaki, and Y. Ikemoto, J. Phys.: Conf. Ser. **592**, 012001 (2015).

⁵² To make the plots, the following data have been used. $\gamma=290$ mJ/K²mol for CeCoIn₅ at 0 GPa,⁵⁰ $\gamma_0=10$ mJ/K²mol for LaCoIn₅,⁵³ $\gamma=382$ mJ/K²mol for CeRhIn₅ at 2 GPa,⁵⁴ and $\gamma_0=5.7$ mJ/K²mol for LaRhIn₅.²⁷

⁵³ S. Nakatsuji, unpublished data.

⁵⁴ R. A. Fisher, F. Bouquet, N. E. Phillips, M. F. Hundley, P. G. Pagliuso, J. L. Sarrao, Z. Fisk, and J. D. Thompson, Phys. Rev. B **65**, 224509 (2002)

⁵⁵ H. Okamura, T. Michizawa, T. Nanba, and T. Ebihara, J. Phys. Soc. Jpn. **73**, 2045 (2004).

⁵⁶ In Ref. 36, only the magnetic part of the resistivity (ρ_m) at high P is reported. Therefore, we used the resistivity of LuNi_3Ga_9 at $P=0$ (Ref. 34) as the non-magnetic part (ρ_0) to obtain the total resistivity $\rho = \rho_0 + \rho_m$, and the corresponding dc conductivity. In addition, ρ_m data at 3 GPa are not given in Ref. 36, so we estimated ρ_m at 3 GPa based on the data at $P=0$, 4, and 6 GPa given in Ref. 36.

⁵⁷ H. Okamura, R. Kitamura, M. Matsunami, H. Sugawara, H. Harima, H. Sato, T. Moriwaki, Y. Ikemoto, T. Nanba, J. Phys. Soc. Jpn. **80**, 084718 (2011).

⁵⁸ T. Iizuka, T. Mizuno, B. H. Min, Y. S. Kwon, S. Kimura, J. Phys. Soc. Jpn. **81**, 043703 (2012).

⁵⁹ $\gamma=80$ and 230 mJ/K²mol at $P=3$ and 6 GPa, respectively,³⁷ were used.

⁶⁰ H. Yamaoka, Y. Yamamoto, E. F. Schwier, F. Honda, Y. Zekko, Y. Ohta, J.-F. Lin, M. Nakatake, H. Iwasawa, M. Arita, K. Shimada, N. Hiraoka, H. Ishii, K.-D. Tsuei, and J. Mizuki, Phys. Rev. B **92**, 235110 (2015).

⁶¹ K. Nishiyama, T. Mito, G. Pristas, T. Koyama, K. Ueda, T. Kohara, S. Gabani, K. Flachbart, H. Fukazawa, Y. Kohori, N. Takeshita, N. Shitsevalova, and H. Ikeda, Phys. Rev. B **93**, 121111(R) (2016).

⁶² J. R. Schrieffer and P. A. Wolff, Phys. Rev. **149**, 491 (1966).

⁶³ This is because the negatively charged surrounding of an Yb or Ce becomes closer to the f electrons at high P , causing more Coulomb repulsion between the f electron and the surrounding. Note that an Yb or Ce is positively charged locally, since it provides a few electrons into the spatially extended c band. Hence the surrounding of an Yb or Ce should be negatively charged locally.

⁶⁴ A. Miyake, F. Honda, R. Settai, K. Shimizu, and Y. Ōnuki, J. Phys. Soc. Jpn. **81**, SB054 (2012).

⁶⁵ C. Dallera, E. Annese, J.-P. Rueff, A. Palenzona, G. Vanko, L. Braicovich, A. Shukla, and M. Grioni, Phys. Rev. B **68**, 245114 (2003).

⁶⁶ H. Okamura, M. Nagata, A. Tsubouchi, Y. Ōnuki, Y. Ikemoto, and T. Moriwaki, arXiv:1909.11857.